Ongoing Computational Analysis of Hydroxyl (OH) maser W3(OH)

Grace Zhanel
Independent Study
November 20, 2026

***Abstract*—**I analyze a public 506-second raw voltage (IQ) recording of the 1665 MHz ground-state hydroxyl (OH) line toward the massive star-forming region W3(OH), made in two linear polarizations with a single 6.2 m antenna of the Allen Telescope Array [1]. A Python pipeline is built in order to: average windowed FFT power spectra from the 3.9 GB-per-polarization SigMF files, remove the receiver bandpass with a running median, and convert frequency to velocity in the kinematic local standard of rest (LSRK). It removes the receiver bandpass and instrumental gain jumps, cross-correlates the two polarizations to form Stokes parameters, fits Gaussian components to the line profile, and derives a kinematic distance. The pipeline was validated on a synthetic recording with known gain and polarization properties, all of which it recovered. OH maser emission is detected between -46.5 and -44 kms^{-1}, peaking at $v_{\mathrm{LSR}} = -45.2$ kms^{-1} at about 16σ. The noise is within 7% of the radiometer-equation prediction. The profile is described by five components: narrow features at -46.22, -45.20 and -44.13 kms^{-1}, a broad, weak component carrying about a third of the line area, and a tentative narrow feature at -42.68 kms^{-1}. The -46.2 kms^{-1} feature is essentially fully polarized, equally in both feeds. The main feature is significantly stronger in Y than in X ($q = -0.18 \pm 0.02$), and its X–Y phase changes across the line, which shows that it is a blend of components with different polarization. The phases are consistent with, but cannot confirm, a Zeeman pair implying a field of about 2 mG. With tracing W3(OH)'s motion as the main feature, a flat-rotation-curve kinematic distance of ≈ 3.8 kpc disagrees with the 1.95 kpc maser parallax distance [7], which resurfaces the well-known anomalous motion of this part of the Perseus Arm.

1 BACKGROUND

The hydroxyl radical (OH) has four ground-state hyperfine transitions near 18 cm: 1612, 1665, 1667 and 1720 MHz. In the dense gas around young massive stars, the 1665 and 1667 MHz "main lines" are often amplified by maser action. Instead of a broad, smooth line like the 21 cm hydrogen (HI) line, masers appear as a set of very bright, very narrow spectral spikes. Each spike traces a small, coherent region of gas moving at its own line-of-sight velocity. Because OH has a large Zeeman splitting, OH masers are also among the most direct probes of magnetic fields in star-forming regions.

W3(OH) is a very bright, compact HII region within the W3 complex, coincident with OH masers [3] (Fig. 1). It lies in the Perseus spiral arm [7] and is one of the best-studied OH maser sources. Very Long Baseline Array (VLBA) observations have resolved hundreds of individual OH maser spots in it, including dozens of Zeeman pairs, with typical line widths of 0.15–0.38 $\mathrm{km\,s^{-1}}$ [2]. The source is also a benchmark for Galactic structure: its trigonometric parallax places it at 1.95 ± 0.04 kpc. That measurement resolved a long-standing factor-of-two disagreement with kinematic distances and showed that this part of the Perseus Arm has large non-circular ("anomalous") motions [7].

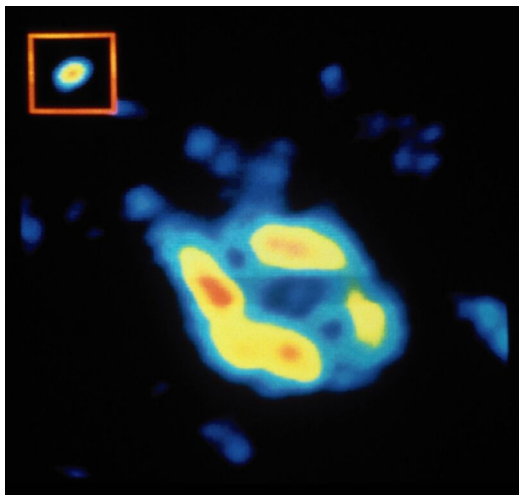


Figure 1—W3(OH) imaged with the Very Large Array in 2 cm (15 GHz) continuum on 1979 February 9 (investigators J. W. Dreher and W. J. Welch). Image: Legacy Astronomical Images, NRAO/AUI Archives [3].

The dataset analyzed here was recorded at the Allen Telescope Array (ATA),

which has been fitted with USRP software-defined radios and a GNU Radio interface to make the array more accessible to people outside the radio astronomy community [6]. The recording was released publicly as raw IQ samples [1], not as finished spectra. Every processing step, from FFT to velocity, therefore has to be done by the user. That makes it a good self-contained exercise in radio spectroscopy, and a stepping stone toward processing my own small-dish observations made with low-cost SDR hardware.

1.1 Methodology

1.1.1 *Change Log*

The first version of this analysis (November 13) produced an averaged, baseline-corrected spectrum and identified the main maser features, but several of its results were qualitative or affected by instrumental effects. The pipeline has since been extended in the following ways:

- **Per-row normalization of the dynamic spectrum.** The waterfall previously divided every 10 s row by a single time-averaged bandpass, so gain jumps in the X channel appeared as bright horizontal bands. Each row is now rescaled to its own gain, the X and Y rows are averaged, and the gain of every row is plotted against time. This exposes the X-channel gain steps directly (see *Per-Row Normalization of the Dynamic Spectrum*).
- **Formal noise measurement.** The rms of the line-free channels was previously estimated by eye at about ± 0.003. It is now measured as a robust standard deviation and compared with the radiometer equation, giving $0.93\times$ the prediction (see *Noise Level and Radiometer Check*).
- **Quantitative line decomposition.** The features were previously described by reading peak positions off the plot. The profile is now fitted with Gaussian components, the number of components is chosen by the BIC, and each component's velocity, peak, width and area are reported with uncertainties. As a result, the "shoulder" near -44.9 kms^{-1} is reinterpreted as a broad, weak component. A tentative narrow component at -42.68 kms^{-1} is also identified (see *Gaussian Decomposition of the Line Profile*).
- **Kinematic distance from the fit.** The distance is now computed from the fitted velocity of the main component. It is plotted against the rotation curve and compared directly with the parallax distance (see *Kinematic Distance*).
- **Full polarization analysis.** Polarization was previously inferred by comparing

the heights of the X and Y profiles by eye. The two polarizations are now cross-correlated to form Stokes I, Q, U and V, with polarization fractions, X–Y phases, a noise-bias correction and empirically measured uncertainties for each feature (see *Stokes Parameters*).

- **Validation on synthetic data.** A synthetic two-polarization recording with a known gain jump and five lines of known polarization was generated with `make_synthetic_test.py`. The pipeline recovered the gain jump and all five polarization states (see *Validation*).
- **Smaller corrections.**
  - A short final row of the dynamic spectrum, which produced a spurious gain drop, is now discarded.
  - Polarization-fraction uncertainties now include the noise in I.
  - The analysis no longer depends on `scipy.signal`, which failed to import on the analysis in this experiment.

1.1.2 *Per-Row Normalization of the Dynamic Spectrum*

The dynamic spectrum is built by averaging the FFT power spectra in consecutive 10 s blocks. Each block forms one row $D_k(f)$, where k is the row index and f the frequency channel. In the first analysis, every row was divided by a single time-averaged bandpass $B(f)$. Any change in the receiver's broadband gain during the recording therefore appeared as a bright or dark horizontal band across all velocity channels. These bands were strongest in the X polarization, where they hid the maser emission in the affected rows.

To remove them, each row is now normalized by its own baseline. I estimate a relative gain for every row as the median, over all usable channels, of the ratio between that row and the time-averaged bandpass:

$$g_k = \underset{f}{\text{median}} \left[\frac{D_k(f)}{B(f)} \right], \tag{1}$$

and each row is normalized as

$$\frac{D_k(f)}{g_k B(f)} - 1. \tag{2}$$

The median makes g_k insensitive to the few channels that contain maser emission. It measures only the broadband level of the row, so a gain jump is divided out while the narrow spectral line is kept. The band edges and the DC spike are excluded from the median, as in the time-averaged analysis. A final row

containing fewer than half the usual number of FFTs is discarded: the median of only a few averaged spectra is biased low, and such a row would otherwise appear as a spurious gain drop.

After normalization, the rows from the X and Y polarizations are averaged channel by channel (truncated to their common length). This produces a single waterfall with higher signal-to-noise and no polarization-specific gain artifacts (Fig. 2, panel 3). The gains g_k, expressed as a percentage change from their median, are plotted against time for each polarization (Fig. 2, panel 4). That makes the instrumental gain variations directly visible rather than embedded in the waterfall, and the range of each polarization's gain variation is reported alongside the plots.

Two other normalization modes were implemented for comparison. In the first, each row is divided by its own 300 kHz running median, the same estimator used for the time-averaged baseline. This also follows changes in the *shape* of the bandpass over time, but is considerably slower. The second keeps the original single time-averaged baseline, so results can be compared directly with the earlier analysis.

1.1.3 *Noise Level and Radiometer Check*

Before fitting, the noise in the baseline-removed spectrum is measured as the rms of line-free channels. It is computed as a robust standard deviation ($1.4826\times$ the median absolute deviation), so that a stray interference spike cannot inflate it. The line-free channels are those between -60 and -50 $\mathrm{km\,s^{-1}}$ and between -40 and -30 $\mathrm{km\,s^{-1}}$, which lie on either side of the maser emission and avoid the band edges and the DC spike. Because Eq. 2 puts the spectrum in units of the baseline, the radiometer equation predicts a per-channel rms of

$$\sigma_{\mathrm{rad}} = \frac{1}{\sqrt{\Delta\nu\, t_{\mathrm{int}}}}, \tag{3}$$

where $\Delta\nu = f_s/N_{\mathrm{FFT}}$ is the channel width and t_{int} the total integration time. Averaging the two independent polarizations lowers this by a further factor of $\sqrt{2}$. The ratio of measured to predicted rms tests whether the spectrum is limited by thermal noise or by residual baseline structure and interference. For this recording, $\Delta\nu = 1.92\ \mathrm{MHz}/16384 = 117.2$ Hz and $t_{\mathrm{int}} = 506.2$ s. The predicted rms of the X+Y average is $1/\sqrt{2 \times 117.2 \times 506.2} = 0.00290$. The measured rms is 0.00270, or $0.93\times$ the radiometer prediction.

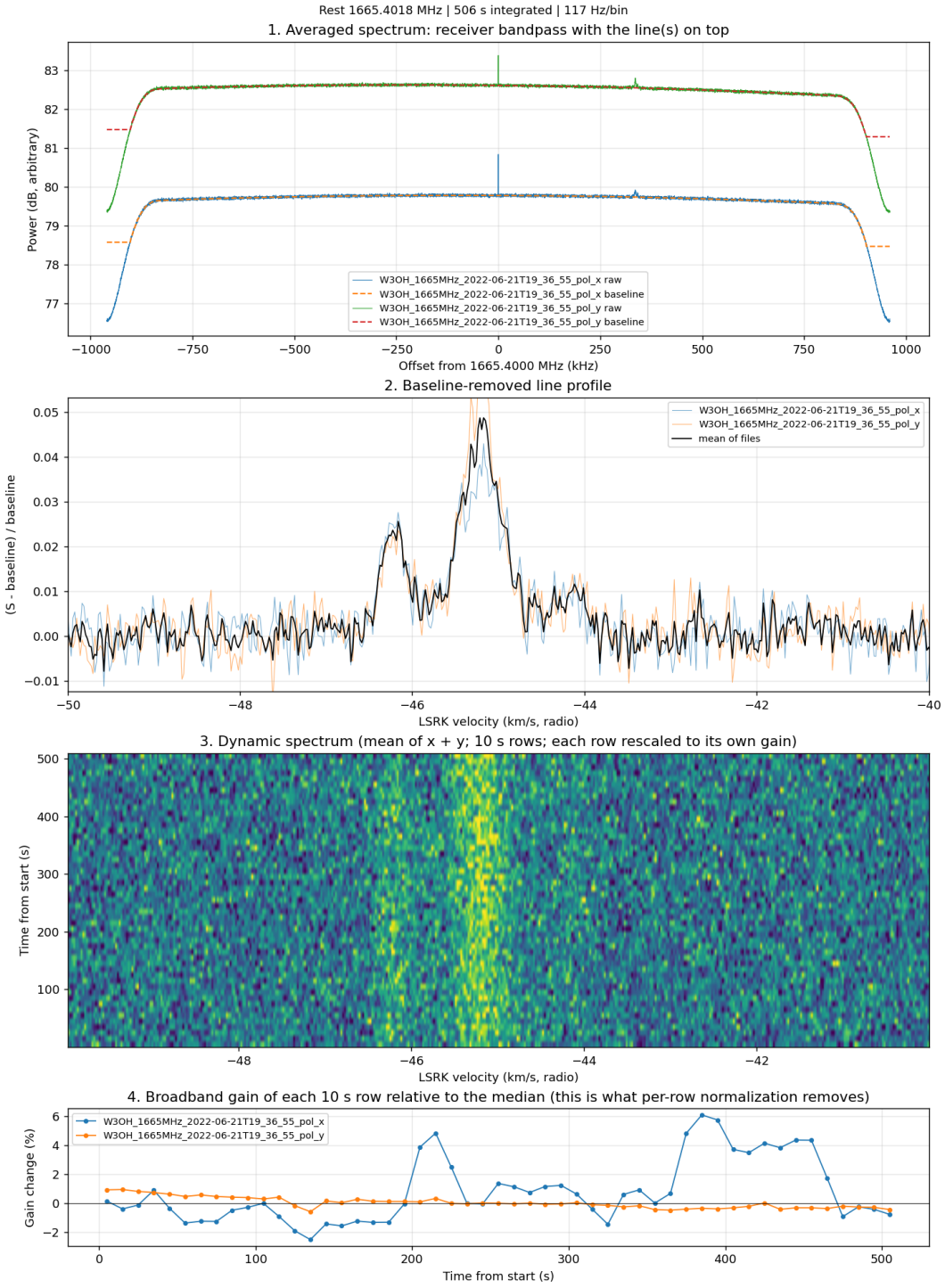


Figure 2—`xy_rows`: (1) raw averaged spectra of both polarizations; (2) baseline-removed line profile; (3) dynamic spectrum, mean of X and Y, with each 10 s row normalized by its own gain (Eq. 2); (4) relative broadband gain of each row for X and Y.

1.1.4 *Gaussian Decomposition of the Line Profile*

The baseline-removed profile (Fig. 2, panel 2) is modelled as a sum of N Gaussian components,

$$S(v) = \sum_{i=1}^{N} A_i \exp\left[-4\ln 2\,\frac{(v - v_i)^2}{\Delta v_i^2}\right], \tag{4}$$

where A_i is the peak, v_i the centre velocity, and Δv_i the full width at half maximum (FWHM) of component i. The fit uses the X+Y average over -48 to -42.5 km s^{-1}, with every channel weighted by the measured rms of 0.00270.

The fit starts from $N = 4$ components, with starting velocities of -46.2, -45.2, -44.9 and -44.1 km s^{-1} read from the profile. Each centre may move up to ± 0.4 km s^{-1} from its starting value, and each FWHM is limited to 0.07–2.5 km s^{-1}. A further component is then placed at the largest positive residual (smoothed over five channels), and the fit is repeated with $N = 5$. The adopted number of components is the one with the lower Bayesian Information Criterion, $\mathrm{BIC} = \chi^2 + k \ln n$, where k is the number of free parameters and n the number of channels. The BIC rewards a better fit but penalizes every added parameter, so an extra component is kept only if it improves the fit by more than chance would.

Parameter uncertainties are the square roots of the diagonal of the covariance matrix of the weighted least-squares fit. These assume independent channels. The Hann window makes neighbouring channels partly correlated, so the quoted uncertainties are lower limits. Any component whose width ends at one of its limits is flagged as poorly constrained. The integrated area of each component is

$$\int S_i \, dv = \sqrt{\frac{\pi}{4\ln 2}}\, A_i \Delta v_i \approx 1.064\, A_i \Delta v_i. \tag{5}$$

The fitted components are listed in Table 1 and shown in Fig. 3; they are also written to `xy_rows_fit.csv`.

Thermal width comparison.—Each fitted FWHM is compared with the thermal Doppler width of OH,

$$\Delta v_{\mathrm{th}} = \sqrt{\frac{8\ln 2\, k_B T}{m_{\mathrm{OH}}}} \approx 0.52 \text{ km s}^{-1} \left(\frac{T}{100\text{ K}}\right)^{1/2}, \tag{6}$$

with $m_{\mathrm{OH}} = 17.0$ u. This was evaluated for $T = 50$, 100 and 150 K, giving 0.37, 0.52 and 0.64 km s^{-1}. A component narrower than the thermal width at a plausible kinetic temperature cannot be thermally broadened gas emission alone, and is consistent with maser amplification, which narrows the line.

Table 1—Gaussian components fitted to the baseline-removed X+Y line profile (`xy_rows_fit.csv`). Velocities are LSRK; peaks and areas are in units of the system noise. Uncertainties are from the fit covariance and are lower limits (see text).

Component	v (kms^{-1})	Peak	FWHM (kms^{-1})	Area (kms^{-1})
1	-46.220 ± 0.008	0.0209 ± 0.0011	0.313 ± 0.022	0.00696
2 (broad)	-45.300 ± 0.082	0.0080 ± 0.0013	1.672 ± 0.220	0.01428
3	-45.197 ± 0.006	0.0376 ± 0.0014	0.481 ± 0.020	0.01925
4	-44.130 ± 0.021	0.0079 ± 0.0011	0.345 ± 0.060	0.00289
5 (tentative)	-42.681 ± 0.018	0.0056 ± 0.0015	0.145 ± 0.043	0.00087

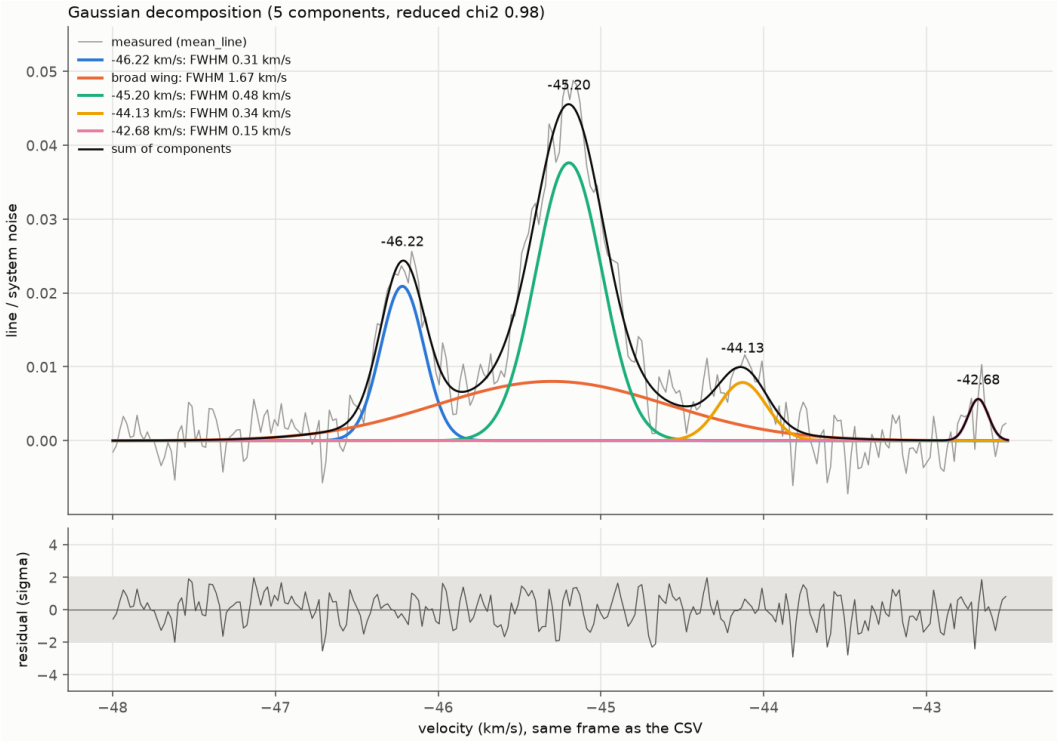


Figure 3—`xy_rows_fit`: top, the baseline-removed X+Y line profile (grey) with the five fitted Gaussian components (coloured) and their sum (black); bottom, the fit residuals in units of the channel rms, with the $\pm 2\sigma$ band shaded.

1.1.5 *Kinematic Distance*

The fitted centre velocities are converted to a distance using a Galactic rotation curve. For a source at Galactic longitude l and latitude b, the line-of-sight velocity relative to the local standard of rest is

$$v_{\mathrm{LSR}} = R_0 \sin l \cos b \left(\frac{\Theta(R)}{R} - \frac{\Theta_0}{R_0} \right), \tag{7}$$

where R is the source's Galactocentric radius, and R_0 and Θ_0 are the Sun's Galactocentric radius and circular velocity. Once R is known, the heliocentric distance d follows from

$$d \cos b = R_0 \cos l \pm \sqrt{R^2 - R_0^2 \sin^2 l}. \tag{8}$$

For $90^\circ < l < 270^\circ$ only the positive root is physical, so the distance is unique. In practice the script evaluates $v_{\mathrm{LSR}}(d)$ along the line of sight and finds where it crosses the measured velocity, which handles both cases without choosing a root by hand. I used a flat rotation curve, $\Theta(R) = \Theta_0$, with $R_0 = 8.15$ kpc and $\Theta_0 = 236$ kms^{-1} [4]. The source position is $(l, b) = (133.95^\circ, 1.06^\circ)$, and $v_{\mathrm{LSR}} = -45.20$ kms^{-1}, the strongest fitted component (component 3 in Table 1). This gives $d = 3.77$ kpc. Kinematic distances assume pure circular rotation. Streaming motions and the offset of maser velocities from the systemic velocity can make them uncertain by 10–20 kms^{-1} in velocity or more. At this longitude, each 1 kms^{-1} of non-circular motion shifts the distance by about 0.1 kpc. For W3(OH) the kinematic distance is known to be wrong by about a factor of two [7], so the result is also compared with the parallax distance of 1.95 kpc.

1.1.6 *Stokes Parameters*

The two linear polarizations are recorded coherently, so the full set of Stokes parameters can be formed from the complex voltages X and Y of each FFT:

$$\begin{aligned} I &= \langle |X|^2 \rangle + \langle |Y|^2 \rangle, & Q &= \langle |X|^2 \rangle - \langle |Y|^2 \rangle, \\ U &= 2\mathrm{Re}\langle XY^* \rangle, & V &= 2\mathrm{Im}\langle XY^* \rangle, \end{aligned} \tag{9}$$

where $\langle \cdot \rangle$ is the average over FFTs. The sign of V follows this definition, which is not tied to the IAU handedness convention. Since the X–Y phase is uncalibrated, the absolute sign of V is not used in this work.

Before forming the Stokes parameters, each auto-power spectrum is divided by its own 300 kHz running-median bandpass (and 1 is subtracted), which removes the Y/X power ratio. The cross-power $\langle XY^* \rangle$ has its own off-line baseline: a

running median of its real and imaginary parts, which captures any correlated receiver noise between the feeds. That baseline is subtracted, and the result is divided by $\sqrt{B_X B_Y}$. Every Stokes parameter is therefore in units of one channel's system noise. Features are found automatically as peaks in I that exceed 6σ after five-channel smoothing. Each Stokes parameter is then summed over ± 0.15 km s^{-1} around each peak, and the polarization fractions are ratios of these sums to the summed I.

The relative phase between the X and Y signal paths is not calibrated. The instrumental phase therefore rotates power between U and V, so the two cannot be separated individually. I report instead the fraction of correlated polarized power, $\sqrt{U^2 + V^2}/I$, together with the phase $\arg\langle XY^* \rangle$. The magnitude is independent of the unknown phase offset, and the phase difference between two lines is meaningful even when the absolute phase is not. Linear polarization along the feeds appears in $q = Q/I$, which requires no phase calibration but assumes equal system temperatures in X and Y. Two lines whose phases differ by 180° have opposite signs of polarization in the (U, V) plane. For lines that are purely circularly polarized, this means opposite circular hands, the signature of a Zeeman pair.

The quantity $\sqrt{U^2 + V^2}$ is a positive-definite combination of noisy terms, so noise biases it upward. A first-order correction is applied: the noise term is subtracted in quadrature, $P_{\mathrm{corr}} = \sqrt{\max(P^2 - \sigma_P^2, 0)}$. Uncertainties on the summed Stokes parameters are measured empirically. Line-free channels are split into blocks of the same width as the feature window, and the robust scatter of the block sums is taken as the uncertainty. This includes the correlation between neighbouring channels that a simple $\sigma\sqrt{n}$ would miss. The uncertainty of each polarization fraction also includes the noise in the summed I. The uncertainty of each phase is σ_P/P in radians.

1.1.7 *Validation*

The method was tested on a synthetic 30 s, two-polarization recording with known properties (Table 2). A 3% step in signal amplitude was inserted into the X channel between 10 and 15 s. Because power scales as amplitude squared, this corresponds to a $1.03^2 - 1 = 6.09\%$ change in power. The recovered row gain was $+6.06\%$ for the affected rows. The Y channel stayed within $\pm 0.15\%$, and no residual band was visible in the normalized waterfall.

The recording also contains five lines with known polarization states. The line polarized along X was recovered with $q = 0.97 \pm 0.05$, and the unpolarized line gave fractions consistent with zero. The lines that put power into U or V gave correlated fractions between 0.97 and 1.13. The two circular lines of opposite hand were recovered 181° apart, against an expected 180°. With the injected instrumental phase offset of −40° left uncalibrated, the measured phases (+49°, −132° and −36°) agree with the expected +50°, −130° and −40° to within 4°. This confirms that phase differences between lines survive the missing calibration.

Table 2—Known properties of the synthetic validation recording (30 s, 1.92 Msps, centred on 1665.4 MHz), generated with `make_synthetic_test.py`.

Property	Value	Recovered
Y/X power ratio	2.92 dB	removed by normalization
X gain jump (10–15 s)	+3% amplitude (+6.09% power)	+6.06%
Y gain variation	none	within ±0.15%
Line A (−42.88 kms^{-1})	linear along X	$q = 0.97 \pm 0.05$
Line E (−43.78 kms^{-1})	linear at 45°	$\sqrt{U^2 + V^2}/I = 0.97 \pm 0.05$
Line B (−44.68 kms^{-1})	circular	$\sqrt{U^2 + V^2}/I = 1.13 \pm 0.06$
Line C (−45.58 kms^{-1})	circular, opposite hand	$\sqrt{U^2 + V^2}/I = 0.98 \pm 0.05$; 181° from B
Line D (−46.48 kms^{-1})	unpolarized	all fractions consistent with 0

1.2 Interpretation

Detection and noise.—After the LSRK correction (+14.94 kms^{-1} at mid-recording, 2022-06-21 19:41 UTC), the averaged X+Y spectrum shows OH emission between about −46.5 and −44 kms^{-1}. The strongest channel is at −45.17 kms^{-1}, with a peak of 0.049 of the system noise, about 16σ. The rms of the line-free channels is 0.93 times the radiometer prediction (Eq. 3). The spectrum is therefore limited by thermal noise: the baseline removal leaves no measurable residual structure, and there is no sign of interference in the line-free regions. Because the measured noise sits slightly below the prediction, the Hann window's correlation between neighbouring channels may be lowering the channel-to-channel scatter a little; this does not change the conclusion.

Instrumental gain variations.—The row gains (Fig. 2, panel 4) show that the two polarizations behaved very differently during the recording. The X channel

varies between −2.5% and +6.1%, with abrupt steps at about 200 s and 370 s and a plateau until about 460 s. The Y channel varies only between −0.6% and +0.9%, as a slow, smooth drift. Abrupt, single-channel steps are characteristic of the receiver electronics rather than the sky: a change in the sky or in the antenna's pointing would affect both feeds. The cause is most likely a gain change in the X signal path, although the data cannot rule out interference that is itself polarized. After per-row normalization the maser appears as a steady vertical stripe for the full 506 s (panel 3). Over this time span the maser emission shows no variability detectable in 10 s rows.

Line components.—Five Gaussian components describe the profile to within the noise (Table 1, Fig. 3). The reduced χ^2 is 0.98, and the residuals lie within $\pm 2\sigma$ with no remaining structure. The BIC prefers five components over four (325.3 against 331.2). The emission resolves into:

- a main component at -45.20 kms^{-1};
- a second narrow component at -46.22 kms^{-1};
- a weak component at -44.13 kms^{-1};
- a broad, weak component (FWHM 1.67 kms^{-1}) centred under the main peak. It carries about a third (32%) of the integrated line area. The "shoulder" near -44.9 kms^{-1} seen in the earlier analysis is better described by this broad component than by a separate narrow line. A plausible interpretation is a blend of many weak maser spots that the single-dish beam cannot separate, but the data cannot distinguish this from other origins;
- a fifth, very narrow component at -42.68 kms^{-1} (0.0056 ± 0.0015, about 3.7σ). It is treated as tentative. When the two polarizations are fitted separately, it appears in Y (about 3.9σ) but not in X. It also falls below the 6σ threshold of the polarization analysis, and lies close to the edge of the fit window. It may be a weak, polarized maser feature or a noise fluctuation.

The narrow components support maser amplification. Components 1, 4 and 5 have FWHMs of 0.31, 0.35 and 0.15 kms^{-1}. If these widths were purely thermal, the gas would have to be colder than about 36, 44 and 8 K respectively, all below the 0.37 kms^{-1} thermal width at 50 K. The main component (0.48 kms^{-1}) is wider than the 0.15–0.38 kms^{-1} widths of individual W3(OH) maser spots measured with the VLBA [2]. That is expected if it is a blend of several spots at similar velocities inside the roughly 2° beam of a 6.2 m antenna.

Polarization.—The Stokes analysis (Fig. 4) detects two features above 6σ in I:

- -46.18 kms^{-1}**:** $\sqrt{U^2+V^2}/I = 1.15 \pm 0.08$, consistent with complete polarization. At the same time $q = +0.06 \pm 0.05$, consistent with zero: the feature is equally strong in X and Y, yet almost all of its power is correlated between them. That is what a strongly circularly polarized maser would produce. Without a phase calibration, however, linear polarization at 45° to the feeds would look the same. A measured fraction slightly above 1 is within 2σ of 1 and most likely reflects noise.
- -45.19 kms^{-1} **(main feature):** $q = -0.18 \pm 0.02$ (7.7σ), so the main feature is significantly stronger in Y than in X. This confirms the X/Y difference first noticed by eye, and the -46.18 kms^{-1} feature, with $q \approx 0$, acts as a control. If the two channels simply had different system temperatures, every feature would show the same non-zero q. The correlated fraction is $\sqrt{U^2+V^2}/I = 0.20 \pm 0.03$ (7.3σ). Together these imply a total polarized fraction of at least $\sqrt{0.18^2+0.20^2} \approx 0.27$.

The channel-by-channel phase (Fig. 4, panel 3) shows that the main feature is not a single polarized line. On its blue side (about -45.5 kms^{-1}) the phase is near 180°, the same as the -46.2 kms^{-1} feature. Across the peak it sweeps through about -90°, reaching about 0° on the red side (about -45.0 kms^{-1}). The main feature is therefore a blend of components with different polarization states. Within the ± 0.15 kms^{-1} measurement window these partly cancel when summed, so the 0.20 correlated fraction is a lower limit for the individual components.

The red side of the main feature is about 180° from the -46.2 kms^{-1} feature, which means opposite signs of polarization. If both are predominantly circular, they would have opposite circular hands. They could then be the two components of a Zeeman pair separated by about 1.2 kms^{-1}. At 1665 MHz the splitting is about 0.59 kms^{-1} per milligauss, so this would correspond to a line-of-sight magnetic field of roughly 2 mG. This remains a hypothesis. A single dish cannot show that the two features come from the same maser spot. The opposite phase could also arise from linear polarization, which cannot be separated from circular without a phase calibration. Zeeman pairs in W3(OH) have been identified securely only with interferometric maps [2].

Kinematic distance.—For the main component, $v_{\mathrm{LSR}} = -45.20$ kms^{-1}, the flat

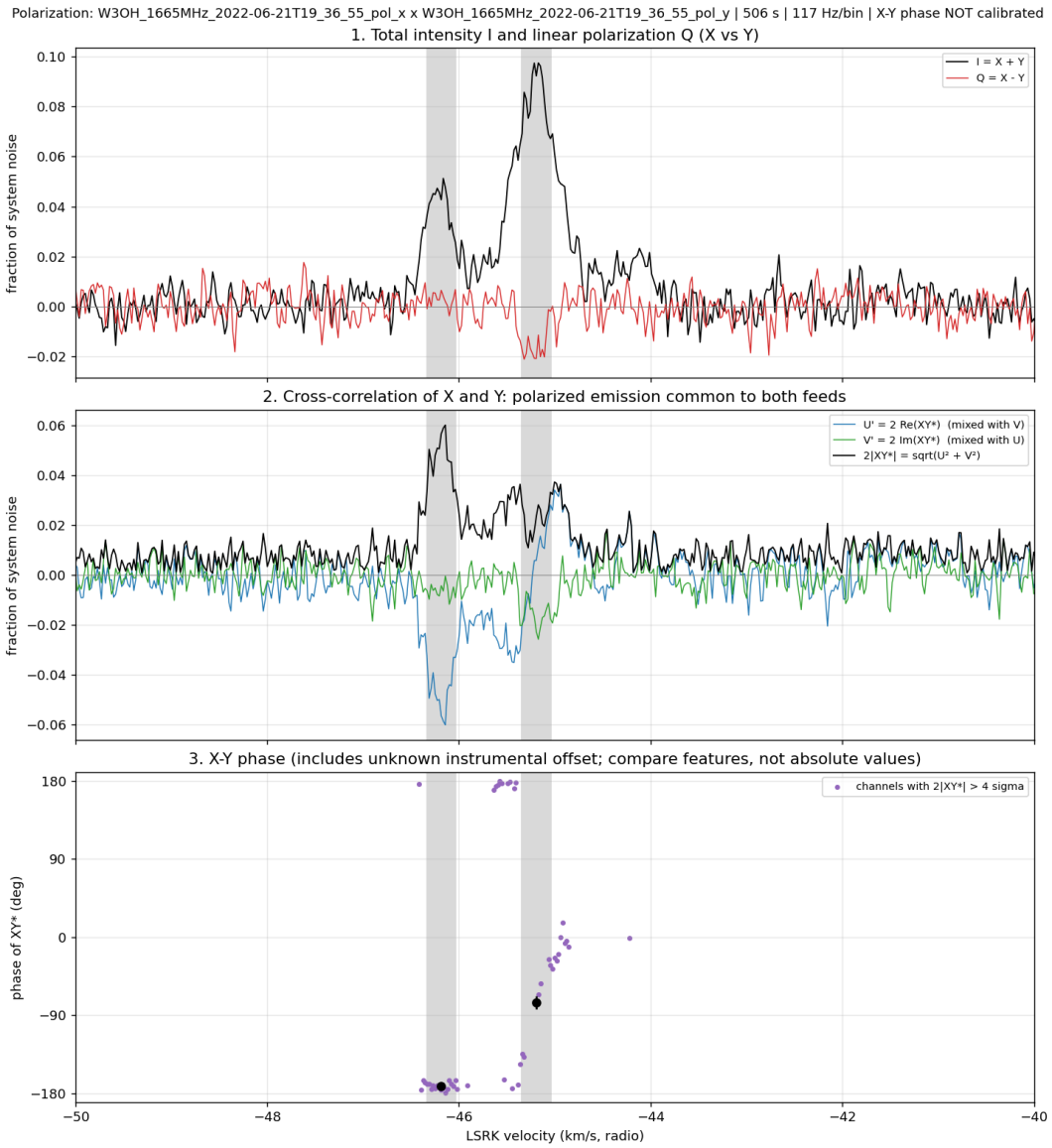


Figure 4—`w3oh_stokes`: (1) Stokes I and Q; (2) the real and imaginary parts of the cross-correlation, U' and V' (mixed by the uncalibrated X–Y phase), and their phase-independent magnitude $\sqrt{U^2 + V^2}$; (3) the X–Y phase of channels with $\sqrt{U^2 + V^2} > 4\sigma$, with the summed value for each detected feature (black). Grey bands mark the ± 0.15 kms^{-1} windows of the two detected features.

rotation curve gives a kinematic distance of 3.77 kpc (Fig. 5). Using any of the other narrow components instead changes this by only about ±0.1 kpc, to 3.67–3.87 kpc. At the parallax distance of 1.95 kpc [7], pure circular rotation predicts $v_{\mathrm{LSR}} = -25.8$ kms^{-1}. The measured velocity therefore differs from circular rotation by about 19 kms^{-1}, nearly doubling the inferred distance. This is not a measurement error. It reproduces the anomalous (non-circular) motion of this part of the Perseus Arm that the parallax measurement revealed [7]. The exact size of the discrepancy depends on the assumed rotation curve and solar motion. It also depends on how well the maser velocities represent the systemic velocity of the region.

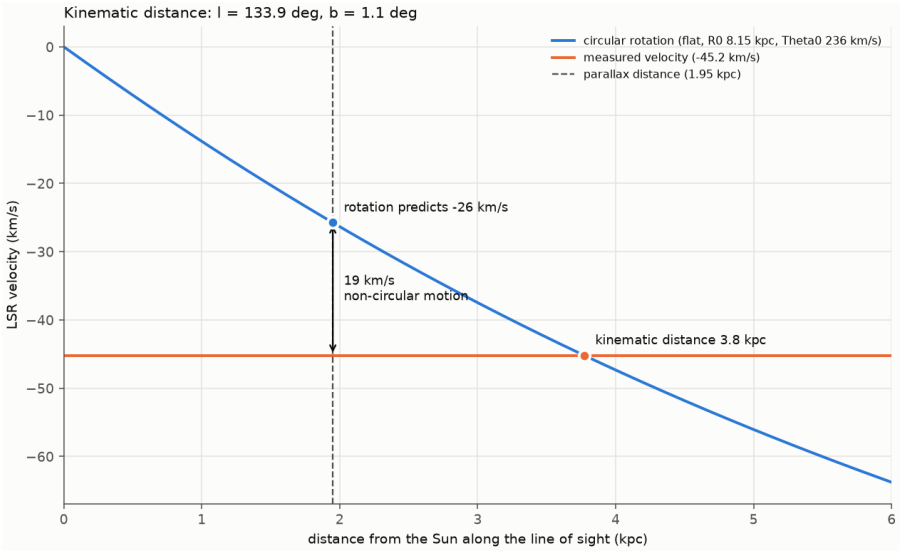


Figure 5—`xy_rows_fit_kinematic`: LSR velocity expected from circular Galactic rotation along the line of sight to W3(OH) (blue), compared with the measured maser velocity (orange) and the parallax distance (dashed).

Limitations.—

- **No flux calibration.** All intensities are relative to the system noise, not in kelvins or janskys, because the system temperature of this antenna is not known here.
- **Single dish.** The ~ 2° beam blends emission from the whole region. Features cannot be assigned to individual maser spots or positions, and some fitted components are probably blends.
- **Uncalibrated polarization.**

  - U and V cannot be separated, so circular and 45°-linear polarization cannot be distinguished.
  - The q measurement assumes equal system temperatures in X and Y. The -46.2 km s^{-1} feature, with $q \approx 0$, partly guards against this.
  - Correlated noise between the feeds at 5% of the system power was found and removed as a baseline. The synthetic test, with independent noise in X and Y, showed only 0.01%, so this correlation comes from the instrument rather than the analysis. If it arises from coupling between the feeds, the same coupling could add spurious polarization of order 0.05 of I. That is small compared with the polarized fraction of the -46.2 km s^{-1} feature (1.15). It is about a quarter of the main feature's 0.20 correlated fraction, so that value is less certain than its statistical error alone suggests.
- **Fit uncertainties.** The Gaussian decomposition is not unique. Its uncertainties are lower limits because neighbouring channels are correlated. Fits to a single polarization are less stable than fits to the X+Y average.
- **Bandwidth.** The 1667 MHz main line is outside the recorded band, so the 1665/1667 line ratio cannot be measured.
- **Assumed time reference.** The start time from the metadata is taken as UTC. A clock error of a few hours would change the LSR correction by at most about 0.2 km s^{-1} (0.4 km s^{-1} for 12 hours), well below the 0.3–0.5 km s^{-1} line widths.
- **Single short epoch.** The recording covers 8.4 minutes on one date, so it cannot test for the month-to-year variability typical of masers.

1.3 Conclusion

Starting from raw IQ samples, a velocity-calibrated, two-polarization spectra of the 1665 MHz OH masers in W3(OH) from 506 s of single-dish ATA data is produced. The emission is detected at about 16σ, and the line-free noise is 0.93 times the radiometer prediction, so the result is limited by thermal noise rather than by residual baseline structure or interference. Per-row normalization showed that the X channel's gain jumped by up to 6% during the recording while the Y channel stayed within 1%. Removing those jumps reveals a maser that is steady over the full recording.

The line profile resolves into five Gaussian components. Their widths, several of them below the thermal width of OH at 50 K, support maser amplification. The main component is wider than individual VLBA maser spots [2], which is consistent with a blend inside the single-dish beam. Cross-correlating the

two polarizations moved the polarization results from visual impressions to measurements:

- the -46.2 km s^{-1} feature is almost entirely polarized;
- the main feature carries a significant linear polarization along the Y feed;
- the main feature's changing X–Y phase shows that it is itself a blend of differently polarized components.

A possible Zeeman pair of about 2 mG remains a hypothesis, because the X–Y phase is uncalibrated and a single dish cannot show that two features come from the same spot. The kinematic distance reproduces the well-known disagreement with W3(OH)'s parallax distance, a direct view of the Perseus Arm's anomalous motion in a spectrum computed from scratch.

Validation on a synthetic recording confirmed that the pipeline recovers known gain jumps, linear and circular polarization, and phase differences between lines, even without phase calibration.

Overall, the exercise shows that public raw-voltage data and a modest open-source pipeline are enough to reach physically meaningful results. That holds as long as the instrumental effects (bandpass, DC spike, gain changes, correlated noise between feeds) and the choice of reference frame are handled carefully and checked against data with known answers.

1.4 Future Direction

- **Polarization calibration.** Separating U from V needs the instrumental X–Y phase. This could come from a recording of a source with known polarization, or from a noise signal injected equally into both feeds, if the ATA can provide either. With V measured directly, the possible Zeeman pair could be tested properly: opposite signs of V at -46.2 and about -45.0 km s^{-1} would support it. The feature velocities could also be compared with the Zeeman pairs mapped in W3(OH) with the VLBA [2].
- **Robustness checks.** Process the two halves of the recording separately (a split-half test) to separate real features from instrumental ones. Plot the noise against integration time to confirm that it keeps falling as $1/\sqrt{t}$.
- **Higher spectral resolution.** Repeat the analysis with 29 Hz channels ($N_{FFT} = 65536$) to see whether the main component splits into narrower parts, and confirm or reject the tentative -42.68 km s^{-1} feature.

- **Variability.** Compare relative feature strengths with other epochs. For example, amateur observers at the Stockert telescope have reported changes in the relative intensity of W3(OH)'s two main 1665 MHz features [5].
- **Own observations.** Apply the same pipeline to my own SDR recordings of the 21 cm hydrogen line, and eventually attempt the W3(OH) 1665 MHz masers with a small dish.

2 REFERENCES

[1] Estévez, Daniel (June 25, 2022). *IQ recording of W3OH hydroxyl spectral line at 1665.4 MHz*. Version v1. Dataset, open access. Zenodo. URL: https://zenodo.org/records/6711078.

[2] Fish, Vincent L., Brisken, Walter F., and Sjouwerman, Loránt O. (Aug. 2006). "A Very High Spectral Resolution Study of Ground-State OH Masers in W3(OH)". In: *The Astrophysical Journal* 647.1, pp. 418–431. DOI: 10.1086/505420. arXiv: astro-ph/0604531.

[3] Legacy Astronomical Images (Feb. 9, 1979). *W3(OH)*. VLA 2 cm (15 GHz) continuum image; investigators J. W. Dreher and W. J. Welch. NRAO/AUI Archives. URL: https://www.nrao.edu/archives/items/show/33495 (visited on 11/14/2026).

[4] Reid, M. J., Menten, K. M., Brunthaler, A., Zheng, X. W., Dame, T. M., Xu, Y., et al. (2019). "Trigonometric Parallaxes of High-mass Star-forming Regions: Our View of the Milky Way". In: *The Astrophysical Journal* 885, p. 131. DOI: 10.3847/1538-4357/ab4a11. arXiv: 1910.03357.

[5] Society of Amateur Radio Astronomers (2025). *OH+ Maser emissions (discussion thread, SARA mailing list)*. URL: https://groups.google.com/g/sara-list/c/l-a5wtdAaUI (visited on 11/13/2026).

[6] White, Ellie, Croft, Steve, Pollak, Alexander W., and Kozel, Derek (2020). "GNU Radio at the Allen Telescope Array". In: *Proceedings of the GNU Radio Conference*. Vol. 5. 1. URL: https://pubs.gnuradio.org/index.php/grcon/article/view/70.

[7] Xu, Y., Reid, M. J., Zheng, X. W., and Menten, K. M. (2006). "The Distance to the Perseus Spiral Arm in the Milky Way". In: *Science* 311.5757, pp. 54–57. DOI: 10.1126/science.1120914. arXiv: astro-ph/0512223.

3 APPENDIX

3.1 Validation Results

This appendix gives the full results of the synthetic validation summarized in the Methodology (Table 2). The synthetic recording has the same format as the ATA data: 16-bit complex samples at 1.92 Msps, centred on 1665.4 MHz, 30 s long. It was generated with a fixed random seed, so it can be reproduced exactly. It contains:

- independent noise in X and Y, shaped by a band-limiting filter;
- a Y-channel power 2.92 dB higher than X;
- an instrumental X–Y phase offset of -40°;
- a 3% amplitude step in X between 10 and 15 s;
- five narrow lines (about 600 Hz wide), each in a different polarization state.

Both analyses were run with the LSR correction disabled, so velocities are topocentric.

Spectrum and gain normalization.—Figure 6 shows the `spectrum` output with 2 s rows. All five lines are recovered at their injected velocities.

- The line polarized along X (line A, -42.88 kms^{-1}) appears only in the X profile, with a peak of 0.32 of the system noise, and is absent from Y.
- The unpolarized line D (-46.49 kms^{-1}) is the strongest in the X+Y average (0.33, about 29σ). It is the only line with full power in *both* polarizations. The other lines split their power between the two feeds or, like line A, put it all in one, so their X+Y averages are about half as high.
- The X-channel gain step is recovered as $+6.06\%$ in the two rows entirely inside the step (against an expected $1.03^2 - 1 = 6.09\%$). It is about $+3\%$ in the row that straddles its end at 15 s, as expected for a row half inside the step.
- The Y channel stays between -0.10% and $+0.14\%$.
- The normalized waterfall (panel 3) shows no band at 10–15 s.

Stokes parameters.—Figure 7 shows the `stokes` output, and Table 3 compares each measured feature with its injected polarization.

- All five lines were found automatically.
- Every measured fraction agrees with its injected value to within about 2σ. The largest deviation is the correlated fraction of the circular line B, at 1.13 ± 0.06

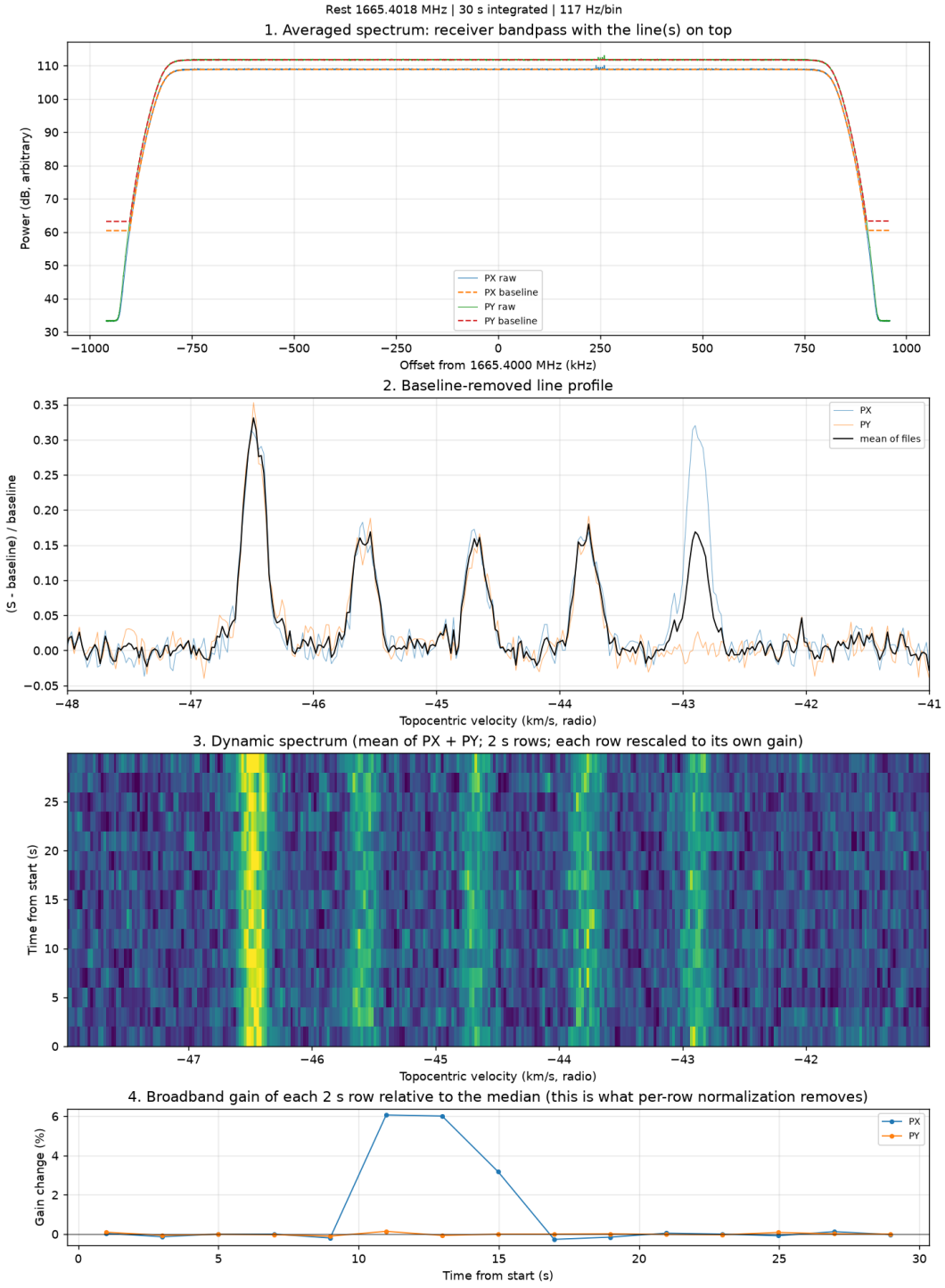


Figure 6—`spectrum` output for the synthetic recording: (1) raw averaged spectra of X and Y, showing the 2.92 dB gain difference; (2) baseline-removed profiles of X, Y and their mean; (3) per-row normalized X+Y waterfall (2 s rows); (4) row gain, showing the injected X-channel step at 10–15 s.

against an expected 1.

- Linear polarization along X appears only in Q (panel 1), and only for line A.
- The three lines with power in U or V appear in the cross-correlation (panel 2), while lines A and D do not.
- The measured phases of lines B, C and E differ from their injected phases by the $-40°$ instrumental offset, to within $4°$. Their phase differences are preserved: C is $181°$ from B (expected $180°$), and E is $96°$ from B and $85°$ from C (expected $90°$).
- The correlated X–Y noise removed as a baseline is 0.0001 of the system power, consistent with the independent noise injected into the two channels. By contrast, the real data showed 0.05. That correlation therefore comes from the instrument, not from the analysis.

Table 3—Polarization of the synthetic lines: injected state and measured values (`stokes`, ± 0.15 km s^{-1} windows, X–Y phase uncalibrated). Expected phases include the injected $-40°$ instrumental offset; "–" means no correlated signal was detected.

Line	v (km s^{-1})	Injected	$q = Q/I$	$\sqrt{U^2+V^2}/I$	Phase (meas./exp.)
D	-46.49	unpolarized	$+0.004 \pm 0.016$	0.021 ± 0.020	– / –
C	-45.58	circular	-0.003 ± 0.030	0.976 ± 0.051	$+49°$ / $+50°$
B	-44.67	circular, opposite hand	$+0.043 \pm 0.034$	1.129 ± 0.062	$-132°$ / $-130°$
E	-43.81	linear at $45°$	$+0.041 \pm 0.031$	0.974 ± 0.053	$-36°$ / $-40°$
A	-42.88	linear along X	$+0.972 \pm 0.050$	0.020 ± 0.041	– / –

Reproducing the validation.—The synthetic data and both analyses are reproduced with:

```
python make_synthetic_test.py --out-dir synth
python oh_spectrum.py spectrum synth/PX.sigmf-meta synth/PY.sigmf-meta
       --no-lsr --vmin -48 --vmax -41 --dump 2
python oh_spectrum.py stokes synth/PX.sigmf-meta synth/PY.sigmf-meta
       --no-lsr --vmin -48 --vmax -41
```

(each `oh_spectrum.py` command is a single line).

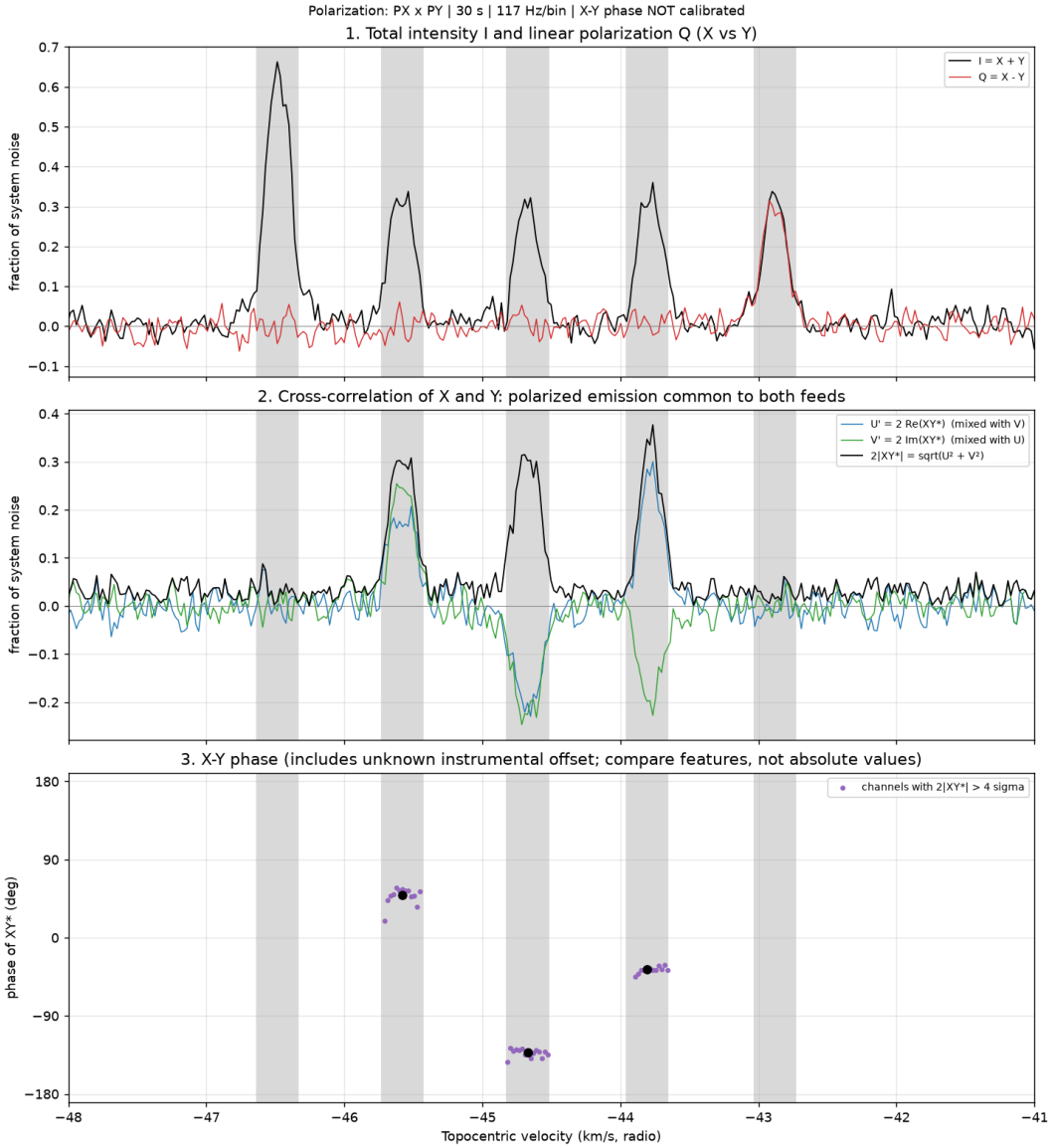


Figure 7—`stokes` output for the synthetic recording: (1) Stokes I and Q; only line A, polarized along X, shows Q; (2) the cross-correlation, where lines E, B and C appear and the unpolarized line D and the X-only line A do not; (3) X–Y phase per channel and per feature (black). Grey bands mark the measurement windows.